United Nations Educational, Scientific and Cultural Organization
Geothermal Training Programme Under the auspices of UNESCO

GRÓ GTP, Urðarhvarf 8,
IS-203 Kópavogur, Iceland

Reports 2022
Number 12

POWER PRODUCTION USING DEEP WELL PUMP AND ORC PLANT IN KOROSI GEOTHERMAL FIELD, KENYA

Dennis K. Chirchir
Geothermal Development Company
17700 - 20100, Nakuru
KENYA
dech@grogtp.is

ABSTRACT

The development of geothermal energy is growing steadily in Kenya with the help of the Kenyan government. However, the exploitation of high temperature geothermal fields has been the focus and utilisation of low to moderate enthalpy geothermal resources utilization for power production has not been widely used. This study proposes the utilisation of a moderate enthalpy well for power production using an electrical submersible pump and an ORC power plant. Modelling and optimization of the ORC plant was done using a custom-made Python model. The proposed setup has an electrical submersible pump with maximum flowrate of 97 kg/s and the ORC plant gives maximum power output of 2,206 kW with thermal efficiencies of 6 – 7.5 %. This model shows a potential to use low to moderate enthalpy geothermal fields for further development to bridge the gap of power requirement in Kenya.

1. INTRODUCTION

Geothermal Development Company (GDC) in Kenya has been mandated with the task to develop geothermal resources in Kenya. This is in line with actualising Kenya's vision 2030 (Vision 2030 website) where the aim is to supply the energy demand for the country through renewable and affordable energy and achieve a middle-income economic status. Kenya's geothermal exploitation has mainly been through power generation at the Kenya electricity generating company (KenGen), which started its activities in the year 1954.

The total installed capacity in Kenya is 2,334 MWe with 1,500 MWe from renewable sources, comprising of geothermal, hydropower, solar, and 836 MWe from fossil fuel. In Kenya, geothermal energy represents 53% of the installed renewable electrical energy, with an installed capacity of 799 MWe by KenGen and plans to increase the capacity is on-going.

Geothermal development takes time to fully mature and be connected to the grid. Conventional steam power plants have a higher efficiency of 10 – 17% compared to binary power plant of 4 – 9 %. Despite having lower efficiencies, binary plant installations are necessary to use low to medium temperature geothermal resources and are key in early power generation.

Kenya, in its quest to supply cheap, reliable, and affordable energy must embrace utilization of low to moderate temperature geothermal resources to generate power and applications in direct use projects.

Kenya's peak power demand rose to 2,117 MW in July 2022, according to the Daily System Operation and Dispatch Analysis Report by Energy and Petroleum Regulatory Authority (EPRA, 2022). With projected growth in power consumption, solutions must be presented and implemented to avoid load shedding which will affect end consumers. Global fuel prices are increasing (EPRA) and are unstable; this leads to high energy prices and subsequently inflation, which greatly affect the consumers at large.

In this study, a technical feasibility of using deep well pump technology combined with a binary power plant to generate power is studied. This setup could potentially be utilised by GDC at drilling sites to substitute use of diesel-powered generators. Consequently, this power could also be used for the surrounding community and subsequent connection to the national grid. Utilisation and successful implementation of this technology could greatly reduce the cost of geothermal exploration and increase the share of geothermal in the energy mix since wells of medium enthalpy have previously not been utilized for power production.

2. REVIEW MATERIAL

2.1 Project Area

Korosi geothermal area is in the northern sector of the actively faulting Kenya Rift Valley, approximately 155 km from the Menengai geothermal project at approximately 177378E and 87696N, as shown in Figure 1. Korosi geothermal field is in the broader Baringo-Silali project funded by the government of Kenya and KfW bank together with Paka and Silali (GDC, 2022). It occupies an estimated area of about 286 km^2 and lies between Eastings 166000 – 193000 and Northings 78000 – 98000. Korosi, unlike many Kenyan volcanoes, is not characterised by a caldera structure but is marked by young volcanism, faulting, and sedimentation that are characteristic of the rift (Njue, 2014). It is located within a shield volcano and the first phase is to develop 100 MWe power plants, and three wells have been drilled to date.

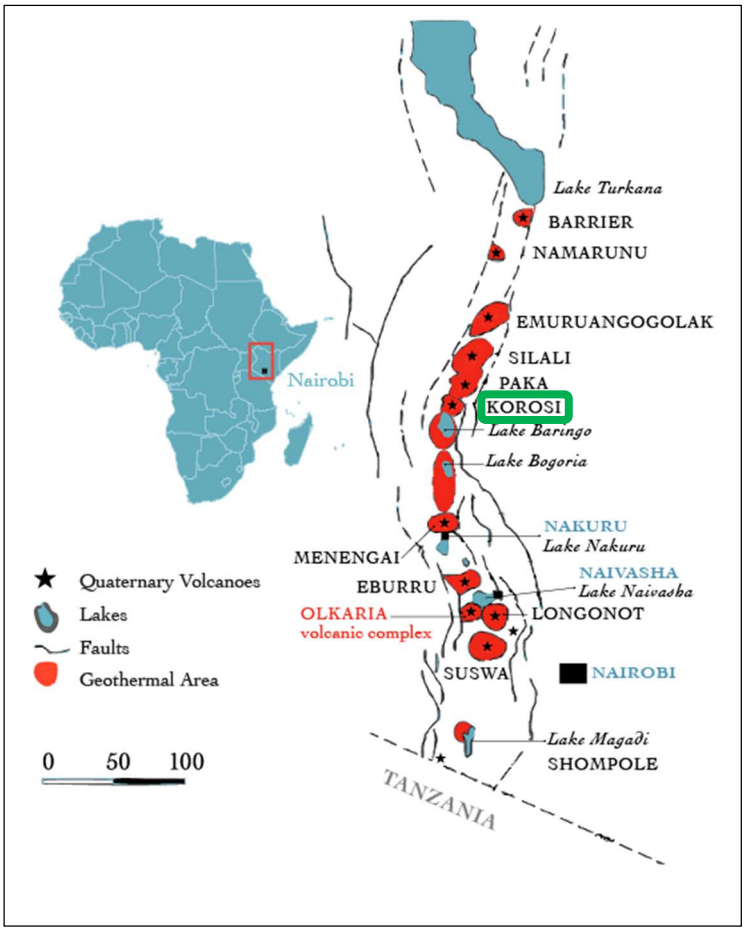

FIGURE 1: Map showing location of Korosi geothermal prospect in green (Lagat, 2004)

The primary geothermal manifestations are fumaroles and changed landscapes. Surface investigations for this project began in 2010 and drilling started 2020. Korosi is part of the phase one project to develop 300 MW power production, and including Paka and Silali, all contributing 100 MW to the project.

2.1.1 Well KW-03

KW-03 is the third exploration well drilled in Korosi geothermal prospect area. It is a vertical well with a slight deviation at 500 m. The total drilled is 1,511 m. The completion test report indicates the main productive region is between 761 – 1,511 m depth with the major feed zone at around 850 m and injectivity rates of 555 L/min per bar, which is a good indication of good permeability and good connection between the wellbore and the reservoir. The location of well KW-03 is shown in Figure 2.

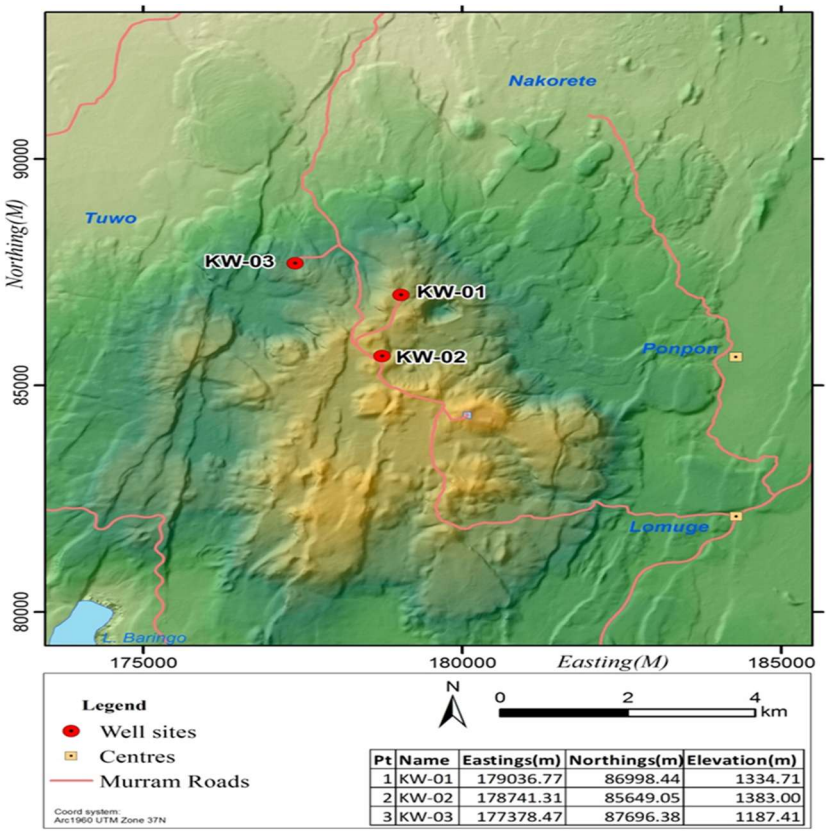

Pt	Name	Eastings(m)	Northings(m)	Elevation(m)
1	KW-01	179036.77	86998.44	1334.71
2	KW-02	178741.31	85649.05	1383.00
3	KW-03	177378.47	87696.38	1187.41

FIGURE 2: Map showing location of wells in Korosi

KW-01 and KW-02 have a lower injectivity compared to KW-03, thus not considered for the study. Downhole temperature and pressure profiles are attached in Figure 3. Static water rest level is between 300 – 320 m and zero wellhead pressure.

Installation of pumps inside the well is dependent on the size of the well. The minimum diameter required for installation of pumps is 9⅝ inches in diameter. Table 1 shows the casing data for KW-03.

A resource with a temperature of less than 150°C is considered a low-temperature resource. These resources can be used for heat pumps or direct use application. Resources with temperatures ranging from 150 to 200°C are moderate or intermediate temperature resources. These intermediate resources can be used for electricity generation, but the wells might require pumping as these wells are not capable of producing large quantities of fluids that are required for large scale electric production (DiPippo, 2016).

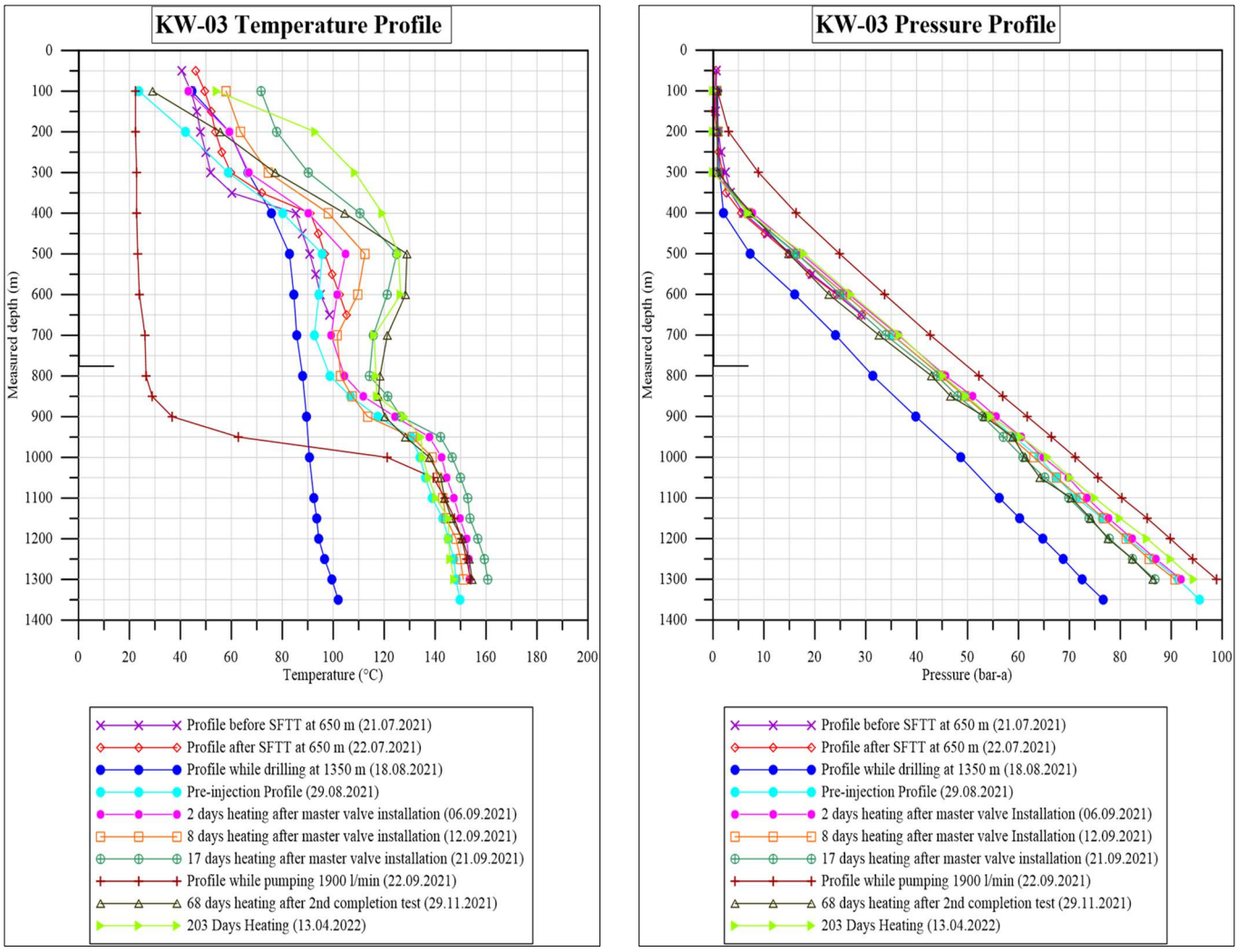

FIGURE 3: KW-03 temperature and pressure downhole profiles

TABLE 1: KW-03 casing data

Well Section	Open Hole diameter (inches)	Casing outer diameter (inches)	Setting depth (meters)	Nominal weight (pound per foot-PPF)	Burst Pressure (Mpa)
Surface	26	20	55.84	104.5	14.5
Intermediate	17 ½	13 ⅜	324	54.5	23.8
Production	12 ¼	9 ⅝	761	47	32.5
Liners landing	8 ½	7	1453	26	

Based on temperature, geothermal resources are classified into three categories. Gehringer and Loksha, (2012) outline the classifications and their possible applications, as shown in Table 2.

TABLE 2: Classification of geothermal resources (Gehringer and Loksha, 2012)

Resource	Temperature (°C)	Use
Low enthalpy	<150	Power generation with binary and direct uses
Medium enthalpy	150 – 200	Power generation with binary power plants and direct uses
High enthalpy	>200	Power generation with conventional steam, flash, double flash

2.2 Deep Well Pump

The development of reliable downhole pumps began in the 1970s when the first binary plants were introduced commercially. Since binary plants generally exploit low to medium temperature geothermal resources that normally cannot be produced without pumping, binary plants could not be effectively operated until pumps could be depended upon to provide long service times (DiPippo, 2015). Downhole pumps and binary plants play a key role in the production of electricity from geothermal reservoirs of moderate and low temperature (and pressures) (Ichikawa et al., 2000; DiPippo, 2005). Advancement of technology has brought two methods of extracting geothermal fluids using deep well pump technology with line shaft mechanical pumps (LSP) or electrical submersible pumps (ESP) (Table 3).

TABLE 3: Comparison between line shaft and electrical submersible pumps (Culver and Rafferty, 1998)

Line Shaft Pump	Electrical Submersible Pump
Lower head/stage and flow/unit diameter.	Higher head/stage and flow/unit diameter.
Usually lower speeds. Lower wear rate	Generally higher speeds, higher wear rate
Higher motor efficiency because it operates in air. Small losses in power cable.	Lower motor efficiency because it operates in oil at elevated temperature. Higher losses in power cable.
Higher temperature capability, up to +200°C.	Lower temperature capability 80-180°C.
Shallower depth settings, commercial app. 280 -300 m, maximum 600 m.	Deeper settings, up to 3600 m in oil wells.
Well must be relatively straight or oversized to accommodate stiff pump and column.	Can be installed in crooked/deviated wells up to 4 degrees deviation per 30 m. Up to 75 degrees off vertical. If it can be cased, it can be pumped.
Easy to use variable speed drives over the whole speed range.	Limited possibility to use variable speed drives.
Impeller position must be adjusted at initial start-up.	Impeller position set.
Easy to maintain locally, motor, thrust bearings and seal accessible at the surface.	Local maintenance hard due to inaccessibility of motor, thrust bearing, seal, and power cable in well.
Longer installation and pump pull time.	Less installation and pump pull time.

Modern pump technology provides more options to explore in geothermal exploitation as they can withstand different geothermal conditions and maintain a high performance for a long time.

2.3 Binary Power Plants

A binary cycle is described as a process where heat is transferred from a primary fluid (e.g., geothermal fluid) to a pressurized secondary/working fluid, which is then directed to a turbine to produce power. The cycle widely used in geothermal application is the ORC cycle. Figure 4 shows a conventional schematic diagram of an ORC plant installation. The green line represents the working fluid, and the red line represents the pumped geothermal fluid. The numbers between 1 – 10 and S1 – S3, represent different thermodynamic state points of the source and working fluid in the thermodynamic cycle. In

this model, geothermal fluid or source fluid is extracted from the well by use of a downhole pump at thermodynamic state S1. Heat is transferred from the geothermal fluid to the pressurised working fluid in the evaporator and the pre-heater to attain states 6 and 3, respectively. The source fluid is then re-injected to the reservoir with thermodynamic properties at S3. The vapourised working fluid is then circulated to the turbine coupled with a generator where it is expanded to generate electrical power between states 6-7. The vapourised working fluid exits the turbine and flows through a recuperator where the unutilised heat energy is transferred to the working fluid circulating from the feed pump. The working fluid then flows through the (air) condenser where it is cooled down and then re-pressurised through the feed pump. A binary cycle system with a recuperator is shown in Figure 4.

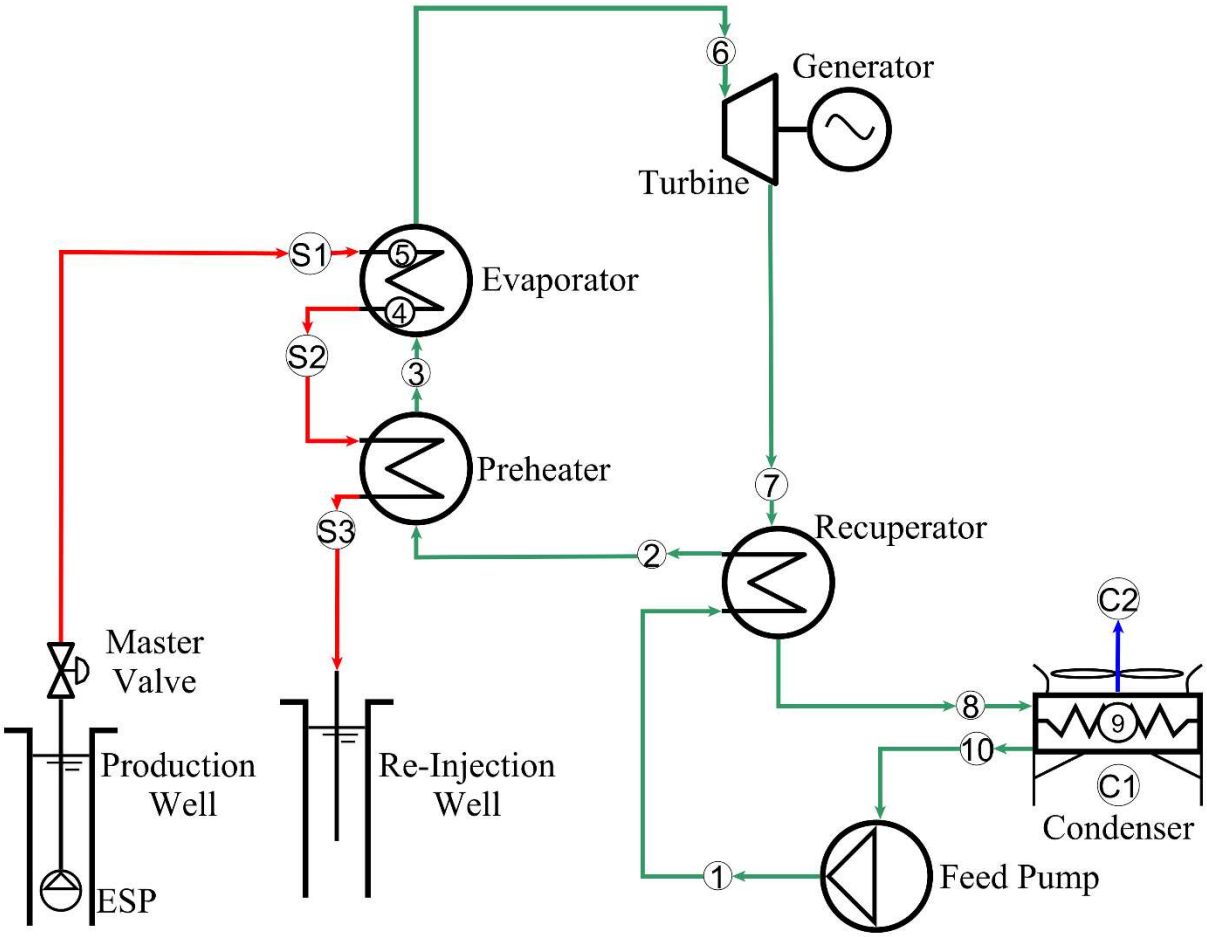

FIGURE 4: Binary plant schematic diagram

2.3.1 Thermodynamic Processes

The thermodynamic processes and fluid states is shown in the T-s diagram in Figure 5. Pumped geofluid enters the evaporator at S1 and gives off heat to the working fluid and exits at point S3 going to the re-injection well. Steps 1 – 6 involves heat addition to the working fluid in the evaporator, preheater, and recuperator at isobaric conditions. At steps 6 – 7, the working fluid enters the turbine and expands to produce power. Steps 7 – 10 represent heat rejection at the recuperator and condenser. The working fluid is re-pressurised at point 10 – 1. Heat rejection by the working fluid to the cooling fluid in the condenser is represented between points C1 – C2.

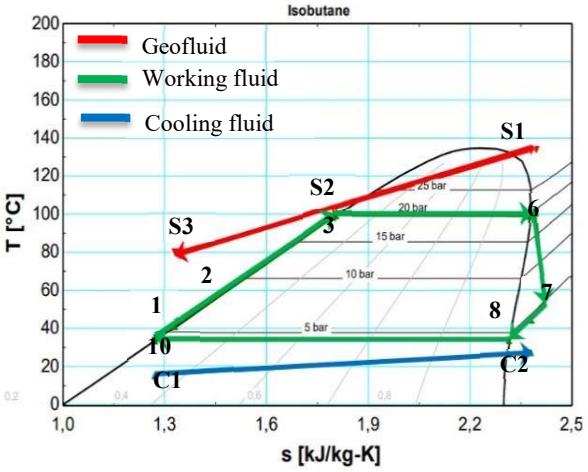

FIGURE 5: T-s diagram of thermodynamic processes

3. METHODOLOGY

3.1 Deep Well Pump

Installation of downhole pumps is for utilization of low – medium temperature resources is increasing and has accelerated power production. Major challenges experienced with previous installations are the boiling of the geofluid leading to corrosion and scaling in the pipe, these can be mitigated by pumping at high pressures. Selecting the correct downhole pump for use must be carefully considered to prevent failure of any project. According to a study by Mwawasi (2014) factors to consider during the selection of a deep well pump include:

- Well size;
- Well deviation;
- Well temperature;
- Power consumption costs;
- Lowest life cycle costs;
- Repair costs;
- Availability of spare parts; and
- Downtime costs.

After the selection of the downhole pump, focus is set on the setting depth as this will affect pump performance and reliability. These different parameters are discussed in the section below.

3.1.1 Factors Affecting Pump Setting Depth

3.1.1.1 Cavitation

Cavitation is the accumulation of bubbles around the pump impeller. When the impeller hits these bubbles, it causes erosion and affects the pump performance. Cavitation causes noise, vibrations, and reduction in flow rate. To avoid this, the minimum pressure setting known as the required net positive suction head (RNPSH), is usually given by the pump manufacturers.

3.1.1.2 Well Inflow Performance

This is a pressure-based test that is used to check the permeability and connection between the wellbore and reservoir. Tests done are injectivity and pressure fall off tests. In this study these tests were done as part of the completion test of the well and the results indicate a good permeability of the well.

3.1.1.3 Flashing Pressure Effects

Flashing occurs when geothermal fluid is exposed to an area with lower pressure and leads to formation of bubbles of dissolved gases. When flashing occurs, the geofluid changes in terms of chemistry and deposition of dissolved minerals can occur. Deposition is mainly calcite scaling and mitigation measures must be put in place to avoid this scenario, either by injecting anti-scaling chemicals in the well or maintaining high pressures. To avoid this, the pressure of the geofluid must be maintained above the flashing pressure and in the case of downhole pumps, this can be achieved by pumping the fluid above the required pressure. Carbon dioxide (CO_2) represents more than 90% of the NCGs in geothermal systems (Nicholson, 1993) and has an important effect on the boiling point-to-depth relationship of the hot fluids (Mahon et al., 1980**).**

3.1.2 Pump Setting Depth Calculation

Figure 6 shows a typical set up of a line shaft pump installation. The dimensions shown in the figure will be used as a reference point to the equations used to calculate the pump setting depth. The calculations apply for both the LSP and ESP.

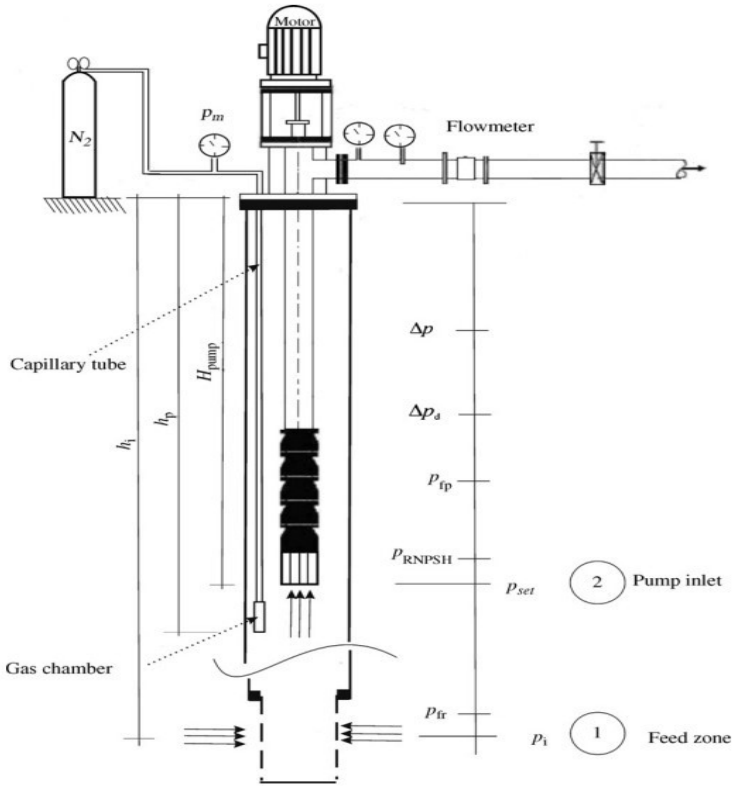

Figure 6: Line shaft pump installation (Aksoy, 2007)

The pressure changes between points 1 and 2, caused by potential differences and friction losses is expressed as:

$$p_1 - p_2 = \rho_b g(h_2 - h_1) + p_{fr} \quad (1)$$

where p_1 = pressure at feed zone;
p_2 = pressure at pump inlet;
ρ_b = geothermal fluid density (kg/m^3);
p_{fr} = friction loss;
h_2 = pump inlet depth; and
h_1 = feed zone depth.

Pressure at the bottom of the capillary tube is expressed as:

$$p_p = p_m + \rho_g g h_p \quad (2)$$

where p_p = pressure at bottom of capillary tube (Pa);
p_m = measured pressure (Pa);
ρ_g = gas density (kg/m^3);
g = gravity acceleration (9.81 m/s^2); and
h_p = depth of end of capillary tube (m).

But pressure at the bottom end of the capillary tube is negligible, thus equation 2 becomes:

$$p_p = p_m \quad (3)$$

Therefore, calculating the pressure change between depth h_i and h_p

$$p_{wf} = p_m + (h_i - h_p)\, \rho_b g + p_{fr} \quad (4)$$

where h_i = average feed zone depth (m); and
p_{wf} = bottom hole flowing pressure (Pa).

However, p_{fr} is the friction loss given by

$$p_{fr} = ((8 f \rho_b q^2)/(\pi^2 D^5)) * (h_1 - h_2) \quad (5)$$

where q = production rate (m3/s);
D = well casing inside diameter (m); and
f = friction factor (dimensionless).

The minimum pump inlet pressure is:

$$p_{in} \geq pRNPSH + p_{fr} \quad (6)$$

where pRNPSH = required net positive suction head (Pa).

The pRNPSH is given by the pump manufacturer. However, during operation drawdown of the reservoir will occur and must be taken into consideration. Thus, the pressure at pump setting depth is given by:

$$p_{set} = p_{min} + \Delta p_d \quad (7)$$

where p_{set} = reservoir pressure at pump set depth (Pa);
p_{min} =minimum pressure at pump depth (Pa); and
Δp_d =estimated reservoir pressure change (Pa).

Rewriting Equation 1 for flow between the feed zone and the pump inlet depth gives:

$$p_{set} = p_{wf} - (h_i - h_{pump})\rho_b g - p_{fr} \quad (8)$$

where p_{wf} = bottomhole flowing pressure (Pa).

Combining equations 6,7 and 8 we get the pump setting for maximum pump flow given by:

$$h_{pump} = (p_{fr} + pRNPSH + p_{fp} + p_d - p_{wf})/\rho_b g) + h_i \quad (9)$$

where h_{pump} = pump set depth (m).

3.2 Binary Power Plant Cycle

A binary power plant set up comprises of heat exchangers, pumps, condenser, and working fluid, as shown in Figure 4. These are key equipment in operation of a binary power plant and are discussed in this section. The thermodynamic equations are given with respect to each equipment.

3.2.1 Working Fluid

Selection of a working fluid is a critical aspect of a binary power plant as this will affect the performance and the output of the plant. Since the critical pressures are reasonably low, it is feasible to consider super critical cycles for working fluid as this reduces the thermodynamic losses in the heat exchangers (DiPippo, 2016). Other factors are flammability, toxicity, chemical aggressiveness, potential hazards to the environment, cost, and availability (Andal, 2019). Table 4 shows some commonly used working fluid properties; pure water is included for comparison (DiPippo, 2016).

TABLE 4: Working fluid properties

Working Fluid	Critical temperature (°C)	Critical Pressure (bar-a)	Toxicity	Flammability
Isopentane	187.8	34.09	Low	Very high
n-pentane	193.9	32.40	Low	Very high
Isobutane	135.9	36.85	Low	Very high
n-butane	150.8	37.18	Low	Very high
Water	374.1	220.89	Low	Non-flam.

3.2.2 Evaporator and Pre-heater

Evaporator and preheater are heat exchangers where pumped geofluid/source fluid flows through and heat is transferred to the working fluid (Figure 7). The source fluid enters the evaporator at state S1, where the working fluid is heated from saturated liquid state to a saturated vapor state and exits at point 6, flowing to the turbine.
Geofluid enters the preheater at point S2, where unutilized heat energy from the source fluid is further used to bring the working fluid to its boiling point. The geofluid exits at S3 and flows to the re-injection well.

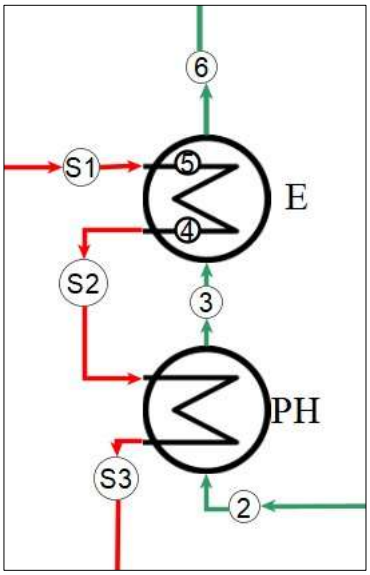

FIGURE 7: Evaporator and preheater

The energy balance of the heat exchangers is given by the following equations:

$$\dot{Q}_E = \dot{m}_{sf} c_p (T_{s1} - T_{s2}) = \dot{m}_{wf} (h_6 - h_3) \quad (10)$$

$$\dot{Q}_{PH} = \dot{m}_{sf} c_p (T_{s2} - T_{s3}) = \dot{m}_{wf} (h_2 - h_1) \quad (11)$$

where: $\dot{Q}_E$ = Heat transfer in the evaporator (kJ);
$\dot{Q}_{PH}$ = Heat transfer in the preheater (kJ);
$\dot{m}_{sf}$ = Mass flow of source fluid/geofluid (kg/s);
$\dot{m}_{wf}$ = mass flow of working fluid (kg/s);
$T_{s..n}$ = temperature at specific state point (°C);
h_n = enthalpy at specific state point (kJ/kg); and
C_P = Specific heat capacity of the geofluid at constant pressure (kJ/kg-°C).

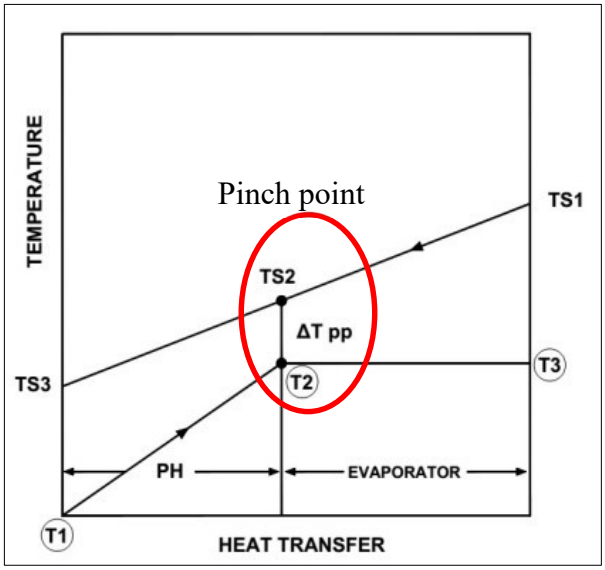

FIGURE 8: Heat transfer diagram in evaporator and preheater

Heat transfer in the heat exchangers is represented in Figure 8. TS1, TS2 and TS3 represent the geofluid temperature as it heats up the working fluid from point TS1 to TS3. The working fluid flows from the preheater to the evaporator from point T1, T2 and T3 respectively.

The minimum temperature difference between the geofluid and the working fluid is known as the pinch point. This is critical as it advices on the design of the heat exchangers specifically on the size/area of the heat exchanger. The value is usually given by the manufacturer. It is represented by the equation below:

$$T_{S2} = T_2 + \Delta T_{pp} \quad (12)$$

where ΔT_{PP} = pinch point temperature difference (°C).

3.2.3 Turbine and Generator

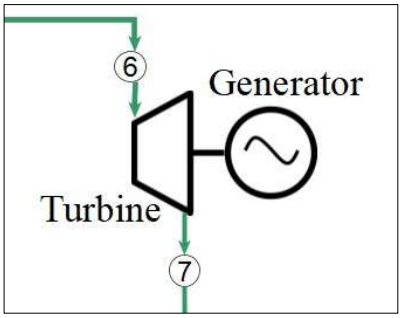

FIGURE 9: Turbine and generator

Figure 9 shows a schematic illustration of a turbine and generator. Pressurised vapor from the evaporator flows to the turbine at state 6, where the thermal energy is converted into mechanical energy and then to electrical energy via the generator. The turbine power output is given by the following equation under ideal conditions:

$$\dot{W}_{Turbine} = \dot{m}_{wf}(h_6\text{-}h_7) \quad (13)$$

However, during expansion of the working fluid losses are observed and must be accounted for to get the actual turbine outlet. The entropy at state 6 equals that at state 7. This is done by getting the turbine efficiency derived from the below equation:

$$\eta_{Turbine} = \frac{h_6 - h_7}{h_6 - h_{s7}} \quad (14)$$

where $\eta_{Turbine}$ = isentropic turbine efficiency; and
h_{s7} = entropy of working fluid at state 7.

Therefore, turbine work power output is given by the following equation respectively:

$$\dot{W}_{Turbine} = \eta_{Turbine} * \dot{m}_{wf}(h_6\text{-}h_{s7}) \quad (15)$$

where $\dot{W}_{Turbine}$ = turbine work output.

3.2.4 Recuperator

A recuperator is a heat exchanger that increases the temperature of the working fluid after condensation and pressurization. Figure 10 shows a schematic illustration of a recuperator. It utilizes the heat energy from the turbine outlet to heat the working fluid from inlet point number 1 and exits at point 2 flowing to the preheater. The energy balance is expressed as:

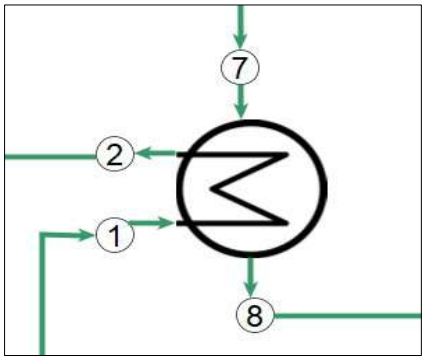

FIGURE 10: Recuperator

$$\dot{Q}_R = \dot{m}_{wf}\,(h_2 - h_1) = \dot{m}_{wf}(h_7 - h_8) \quad (17)$$

where $\dot{Q}_R$ = heat transfer in the recuperator (kJ).

Utilizing recuperative preheaters has the benefit of lessening the heat load on the cooling tower and condenser. The lower capital cost for a smaller condenser and cooling tower must be compared to the extra cost for the recuperators; over the long haul, the resulting higher efficiency should mean lower operating costs.

3.2.5 Condenser

A condenser is a heat exchange equipment that is used for heat rejection. Figure 11 shows an air-cooled condenser used in this model. Working fluid enters the condenser at point 8 where it interacts with cooling fluid. The temperature is reduced until it reaches dew point at point 9, and the vapour becomes saturated liquid. Cooling fluid is either water, air, or a hybrid system. Water-cooled condensers are more practical and cheaper as it utilizes less power in cooling resulting in less parasitic load. Proximity to water source and the environmental temperature conditions are among the factors considered for selection of the cooling tower. Air-cooled condensers are considered in this case for purposes of modelling.

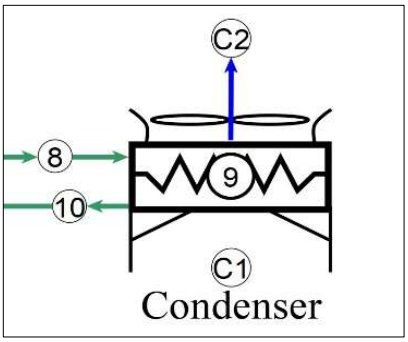

FIGURE 11: Condenser

The heat transfer in the condenser is expressed as follows:

$$\dot{Q}_C = \dot{m}_{air} c_{air}\,(T_{C3} - T_{C1}) = \dot{m}_{wf}(h_9 - h_8) \quad (18)$$

where:
$\dot{Q}_C$ = heat transfer through condenser (kJ);
$\dot{m}_{air}$ = mass of air;
c_{air} = specific heat capacity of air at constant pressure;
T_{C3} = temperature at point C3 (°C); and
T_{C1} = temperature at point C1 (°C).

3.2.6 Feed Pump

The feed pump is used to re-pressurise the working fluid after condensation. Figure 12 shows the working flows into the pump at point 10 from the condenser and exits at point 1 flowing to the recuperator. The work done by the pump is expressed as:

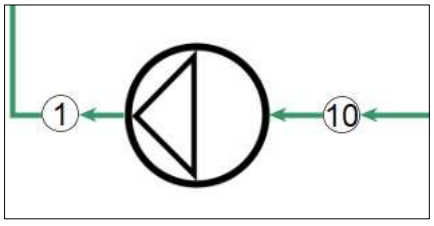

FIGURE 12: Feed Pump.

$$\dot{W}_{feed\ pump} = (\dot{m}_{wf}(h_8 - h_{10}) = \dot{m}_{wf}(h_{8s} - h_{10}))/\,\eta_p \quad (19)$$

where $\dot{W}_{feed\ pump}$ = work done by the feed pump; and
η_p = isentropic pump efficiency.

3.2.7 Heat exchange area

The area of the heat exchangers is calculated using the formula:

$$Q = U*A*(LMTD) \quad (20)$$

$$LMTD = \frac{(T_{hot,in} - T_{cold,out}) - (T_{hot,out} - T_{cold,in})}{\ln\frac{(T_{hot,in} - T_{cold,out})}{(T_{hot,out} - T_{cold,in})}} \quad (21)$$

Where Q = Heat transfer through equipment (J or kJ);
U = Overall heat transfer coefficient (°C/m^2);
A = Heat transfer area (m^2); and
LMTD = Log mean temperature difference (°C)

Heat transfer coefficients for isopentane are assumed (Páll Valdimarsson, adjunct professor at Reykjavík University, pers. comm., 2019 in Andal, 2019), as shown in Table 5.

TABLE 5: Heat transfer coefficients

Process	STAGE	Heat transfer Coefficient U (kW/m^{2}K)
Geothermal heat to isopentane (vapour)	Evaporator	0.8
Geothermal heat to isopentane (boiling)	Evaporator	1.2
Geothermal heat to isopentane (liquid)	Preheater	0.5
Cooling air to isopentane (vapour)	Condenser	0.5
Cooling air to isopentane (dew)	Condenser	1.0
Isopentane vapour to isopentane liquid	Recuperator	0.3

3.2.8 Assessment of Binary Cycle

Thermal efficiency is a measure of the heat energy that is converted to into work. Typical values for geothermal binary plants are 5–18%, depending on the temperature of the geofluid and the design of the plant (DiPippo, 2016). Thermal efficiency of the binary plant is given as:

$$\eta_{Therm} = \frac{W_{net}}{Q_{in}} \quad (22)$$

$$\dot{Q}_{in} = \dot{Q}_E + \dot{Q}_{ph} + \dot{Q}_R \quad (23)$$

$$W_{net} = W_{total} - W_{parasitic} \quad (24)$$

$$W_{parasitic} = \dot{W}_{feed\ pump} + \dot{W}_{fan} + \dot{W}_{downhole\ pump} \quad (25)$$

$\eta_{Thermal}$ = thermal efficiency;
Q_{in} = thermal heat energy supplied to the binary system;
W_{net} = net power output (kW);
W_{total} = total power output of the binary plant;
$W_{parasitic}$ = ´power consumed by all the binary plant equipment;
$\dot{W}_{fan}$ = power consumption by the condenser fan; and
$\dot{W}_{downhole\ pump}$ = power consumption by the downhole pump.

4. RESULTS & DISCUSSION

4.1 Deep Well Pump

Based on Table 3, an electrical submersible pump (ESP) is considered for this proposal because it can be installed at a deeper depth and is easier to install in a deviated well. From this two ESPs were considered that could deliver sufficient flow to the surface. The results of the analysis are shown in Table 6.

TABLE 6: ESP calculations

Pump Type (PMM)	**NT47500**			**NV60500**		
	Minimum	**Optimum**	**Maximum**	**Minimum**	**Optimum**	**Maximum**
Flow Rate (l/s)	69	88	97	83	110	139
Head (m)	406	407	362	608	559	388
Pump Power (kW)	396	467	480	761	869	846
Efficiency (%)	67	72	69	67	71	58
Gross Power from ORC (kW)	1569	2001	2206	1888	2502	3161
Net Power (kW)	**1173**	**1534**	**1726**	**1127**	**1633**	**2315**
% Pump Power utilization (kW)	28%	25%	24%	40%	35%	27%

Table 4 shows that ESP type NT47500 is the best option as it consumes less power from the total power output and the net power output is almost same. It gives a flowrate between 69 – 97 kg/s. The output curves for NT47500 calculated from the Novomet ESP calculator software (Novomet ESP, 2022) are shown in Figure 13.

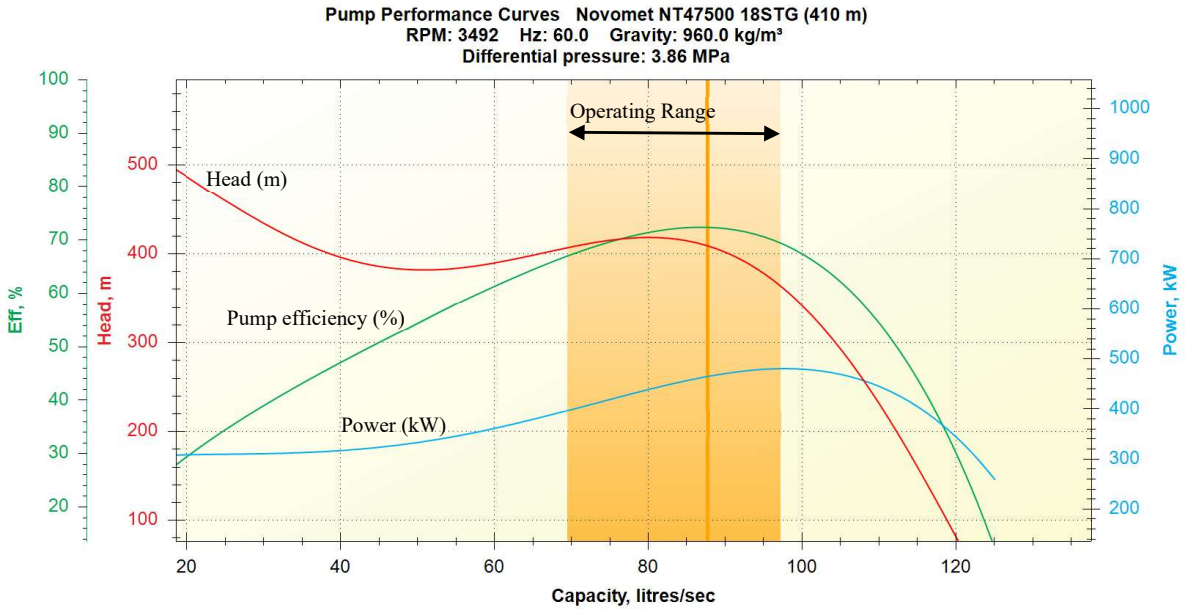

FIGURE 13: Pump performance curves

The operating range for the pump is within the orange space in Figure 13, where the minimum flow rate is 69 l/s and maximum is 97 l/s. Values below or above the operating range lead to wear on the impellers when the pump is operating in either downthrust or upthrust condition.

ESP will use a variable frequency drive that will enable flowrate adjustment, based on the power requirement. This adjustment consequently affects the power consumption of the pump. Figure 14 shows the frequency curves with the corresponding power consumption.

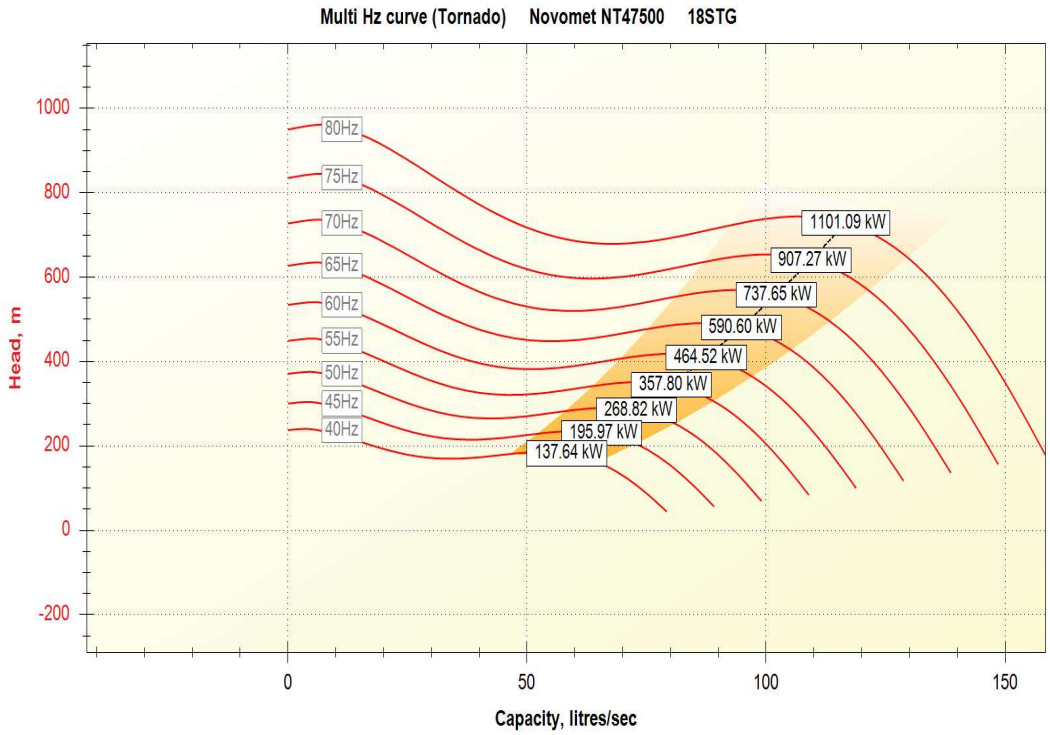

FIGURE 14: Pump frequency curves

The ESP setting depth will be between 450 – 550 m to get maximum output. The depth setting is set based on equations and factors discussed in section 3.1.1.

Minimum operating pressure is 4 bar. The ESP installation in the well is shown in Figure 15. The installation of electrical submersible pump usually takes between 4 – 7 days.

After downhole pump installation, pumping tests must be done to ascertain the well conditions. This usually takes about 2 – 3 days (Lýdur Skúlason, Project manager at HD, pers. comm., July 2022).

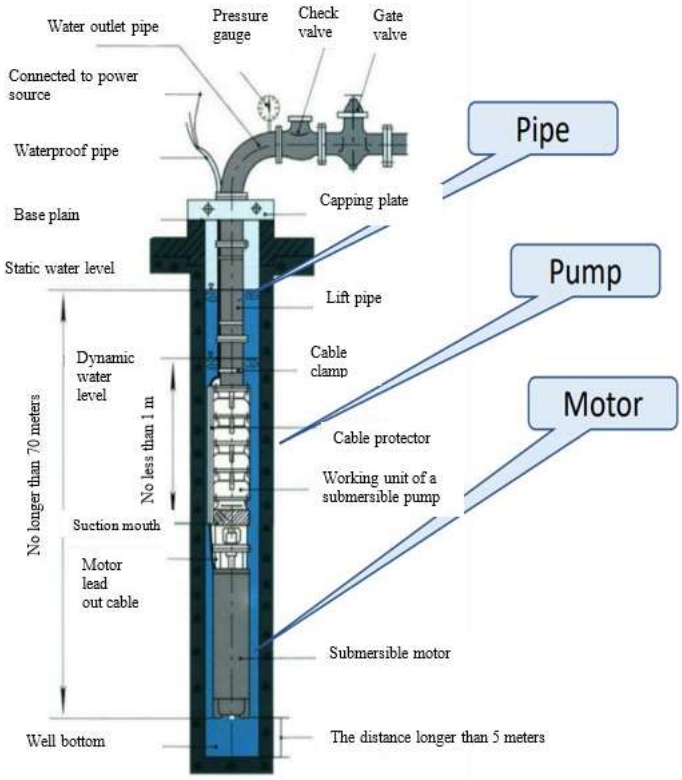

FIGURE 15: ESP installation setup (Lýður Skúlason, Project manager at HD, pers. comm., July 2022)

4.2 Binary Power Plant

4.2.1 Working Fluid Selection

Four working fluids were taken into consideration and the potential power

output is calculated in a python model. The results are presented in the Figure 16 below. Selection of a suitable working fluid for use is critical as it affects the performance of the plant and must be carefully considered. Figure 16 shows the gross output of the four working fluids. Working fluids n-butane and isobutane, shown in Figures 16c and 16d, respectively, give a highest power output but require a high turbine inlet pressure. The high turbine inlet pressure will be supplied by the feed pump, and this requires a big pump installed, which translates to a costly pump, higher parasitic load that reduces the net output.

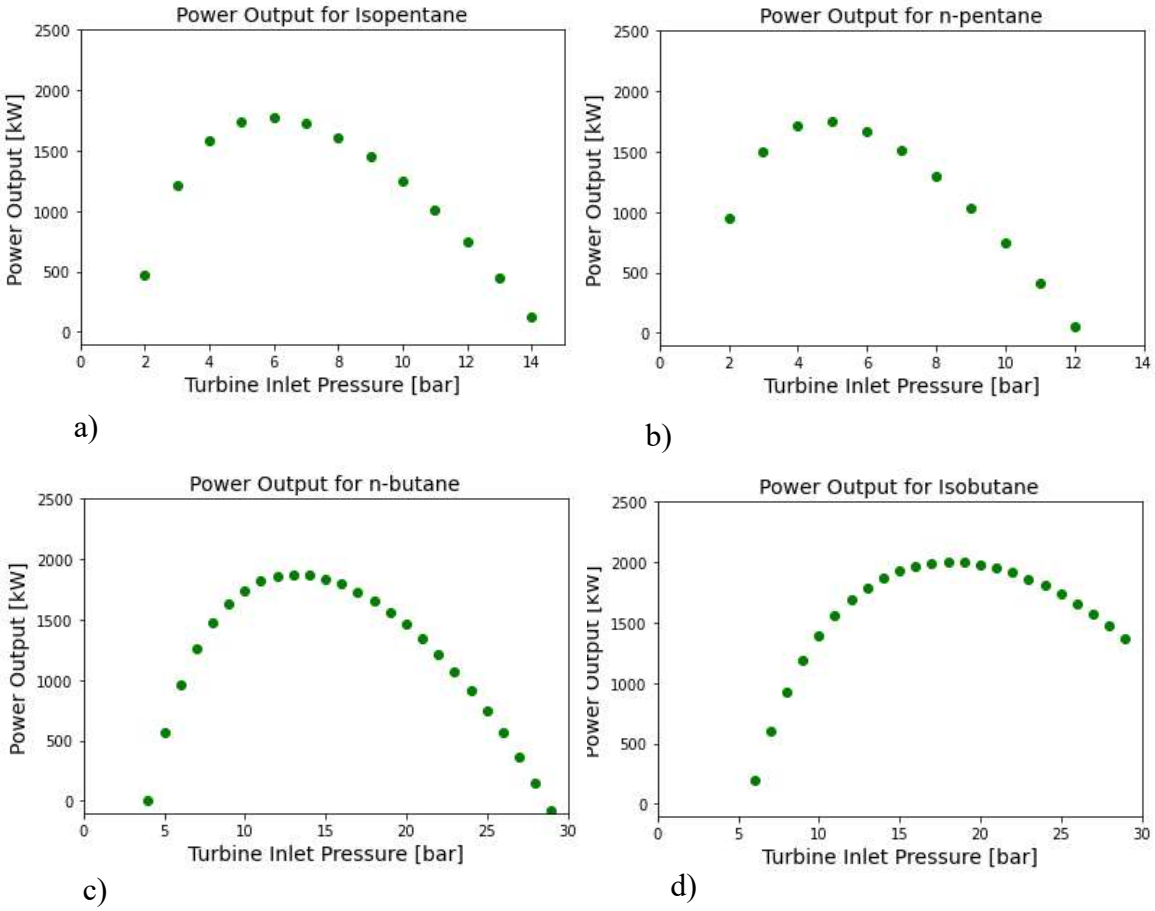

FIGURE 16: Gross power output and turbine inlet pressure for different working fluids

Figures 16a and 16b for isopentane and n-pentane show a slightly lower power output at inlet pressures between 5 – 6 bars. This is achievable and pumps installed will be affordable. Isopentane gross output is the highest and hence selected for use in this study.

4.2.2 Recuperator

A recuperator is installed to improve the thermal efficiency of a binary power plant. This is achieved by reducing the heat load on the condensers. The addition of a recuperator causes no change in the maximum turbine work output of the binary cycle but causes a shift in the maximum point of the turbine work output of the cycle with respect to the reinjection temperature (Figure 17). However, when the reinjection temperature is limited by the geothermal water chemistry, or by other design constraints such as district heating applications, adding a recuperator serves to increase the turbine work output for a given reinjection temperature and helps to overcome these limitations (Monroy, 2013). For this case, the re-injection temperature is not limited. Therefore, a recuperator was not considered for this model.

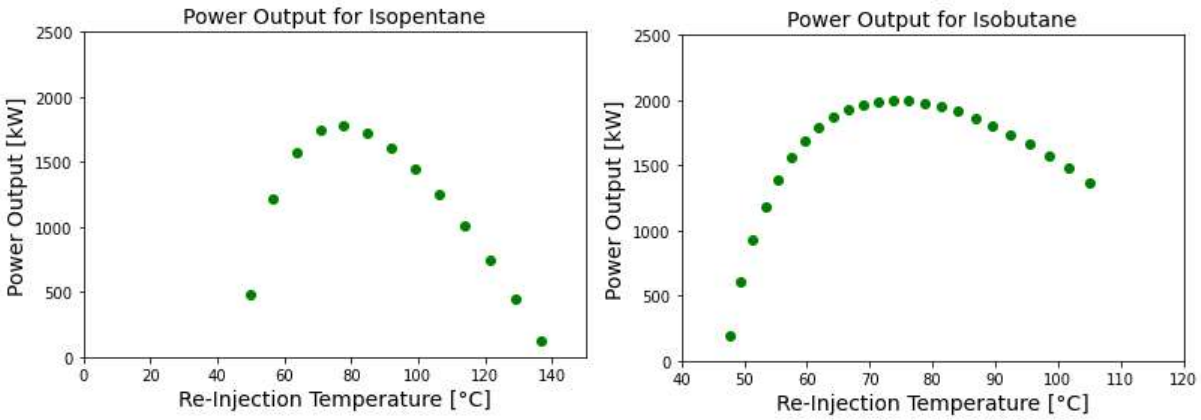

a) b)

FIGURE 17: Power output vs Re-Injection temperature

4.2.3 Binary Power Plant Model

KW-03 model parameters are specified as follows:

TABLE 7: Binary ORC plant input parameters

Description	Value
Working fluid	Isopentane
Temperature of source fluid	140°C
Mass of source fluid	69 kg/s
Wellhead pressure	6 bar-a
Isentropic efficiency of turbine	0.85
Generator efficiency	0.97
Condenser fan efficiency	0.65
Fan motor efficiency	0.98
Pump efficiency	0.75
Ambient air temperature	30°C

Table 7 show the input values for the python model. Assumptions made while setting up the model are listed below:

- Pressure loss in the system due to friction is negligible.
- NCG content is negligible.
- Geothermal fluid has the thermodynamic properties of pure water
- Negligible challenges caused by fluid geochemistry such as scaling.
- Mass of working fluid is constant in the cycle.

Figure 18 shows results calculated based on the minimum flow rate of the electrical submersible pump, using the python model.

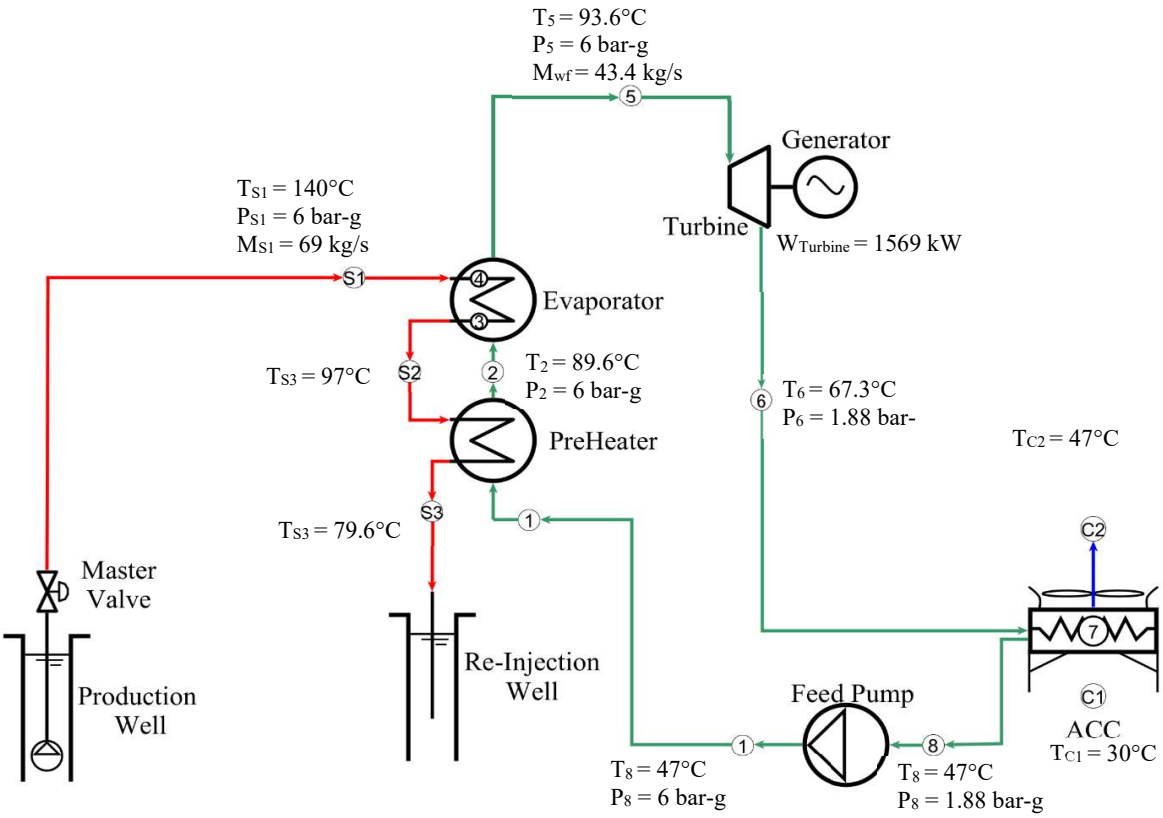

FIGURE 18: Proposed Binary ORC plant

However, based on the pump selection, NT47500, the power output varies based on the flow rates. The results are shown in Table 8.

Table 8: Power output based on different flow rates

Description	Flowrate (l/s)	Gross Power Output (kW)	Parasitic Load (kW)	Net Power Output (kW)	Thermal efficiency
Minimum	69	1569	470	1009	4.9%
Optimal	88	2001	540	1441	6.5%
Maximum	97	2206	560	1646	7.4%

5. FINANCIAL COST ESTIMATION

Investment cost is critical in assessing the viability of any project. In this study cost estimation is done based on the figures provided in Table 9 below:

TABLE 9: Unit cost per equipment
(Dr Páll, pers. Comm, in Andal, 2019).

Component	Unit cost per m^2 or kW
Turbine & generator	400
Heat exchangers	300
Pumps	400

The area of the heat exchangers was calculated based on equations 20 and 21 and costing based on Table 9 used. The cost of the condenser was sourced from an online platform cooling tower depot. The calculations are based on the maximum power output and results are as seen in Table 10:

TABLE 10: Cost for binary power plant equipment

Component	Unit	Unit cost	Total cost (USD)
Evaporator	894 m^2	300	268 200
Preheater	465 m^2	300	139 511
Wet condenser			250 000
Feed pump	29.76 kW	400	11 903
Turbine and generator	2206 kW	400	882 400
Total Cost			1 552 014

The total cost of the above equipment represents approximately 35% of the total cost of binary power plant (David Örn Benediktsson – Verkis Iceland, pers. comm. 2014, in Mwawasi, 2014). This brings the total cost of the binary power plant to 4 434 325 USD. Including the cost of ESP gives a total investment cost of 5 MUSD.

The installation costs are approximately 2.5 MUSD per Mwe which falls within the range that is below the average installation costs of 3.6 MUSD (Ngugi, 2012).

6. CONCLUSIONS

Downhole pumps & binary plants critical in power production and utilization of low – moderate temperature resources.

The model shows that Korosi geothermal prospect, can generate between 1,569 – 2,206 kW electricity based on the mass flow of the geothermal fluid, with a thermal efficiency of 7.4%.

Recuperators do not add the output of the plant. It is necessary to install when there is a temperature limitation on the re-injected geothermal fluid. They not only reduce the workload on the condensers but also the preheater. Therefore, not considered for this model.

Total investment cost is 5 M USD. This is an approximate figure and variance may be seen caused by prevailing market conditions.

Installation costs is 2.5 M USD per MWe.

ACKNOWLEDGEMENTS

I am deeply grateful to my employer Geothermal Development Company for giving me the opportunity to attend this training programme. Special gratitude to the director of GRÓ-GTP, Dr Guðni Axelsson, deputy director Mr. Ingimar G. Haraldsson, operations manager Dr Vigdís Harðardóttir, project manager Málfríður Ómarsdóttir, and Alexander Guðmundsson for their kindness and ensuring my stay in Iceland was smooth. Deeply grateful to my project supervisor assistant professor María Sigríður Guðjónsdóttir and Lýður Skúlason for their invaluable input during all stages of work in the project. Special thanks to Dr Páll Valdimarsson for his support throughout the project.

I would also want to sincerely thank my colleagues in GDC for providing me with the required data to pursue this project. I express my sincere gratitude to the 2022 GRÓ-GTP fellows and the time we shared together.

Finally, I would like to thank my wife and my family for their support during my stay in Iceland.

REFERENCES

Aksoy, N., 2007: *Optimization of downhole pump setting depths in liquid-dominated geothermal systems: A case study on the Balcova-Narlidere field, Turkey.* Torbali Technical Vocational School of Higher Education, Dokuz Eylul University.

Andal, J.M., 2019: Power Plant and Thermo-economics Modelling of Low to Intermediate Temperature Geothermal Resource in Montelago Philippines. *40th Anniversary workshop, UNU-GTP, Iceland.*

Culver, G.G., and Rafferty, K.D., 1998: *Well pumps. In: Lienau, P.J., and Lienau, B.C. (ed), Geothermal direct use engineering and design guidebook (3rd ed.).* Geo-Heat Centre, Oregon Institute of Technology, Klamath Falls, OR, 211-239.

DiPippo, R., 2005: *Geothermal power plants. Principles, applications and case studies.* Elsevier Ltd. Kidlington, UK.

DiPippo, R., 2008: *Geothermal power plants. Principles, applications, case studies and environmental impact.* Elsevier Ltd., Kidlington, UK, 493 pp.

DiPippo, R., 2015: *Geothermal Power Plants, Fourth Edition Principles, Applications, Case Studies, and Environmental Impact.* Elsevier Ltd., Kidlington, UK, 762 pp.

DiPippo, R., 2016: *Geothermal Power generation. Developments and innovation.* Elsevier Ltd., Kidlington, UK.

EPRA, 2022: EPRA company website. *Energy & Petroleum Regulatory authority*, website: *www.epra.co.ke.*

GDC, 2022: GDC company website. *Geothermal Development Company*, website: *www.gdc.co.ke.*

Gehringer, M., and Loksha V., 2012: *Geothermal handbook: planning and financing power generation.* The World Bank, Energy Sector Management Assistance Program, Washington DC, Technical Report 002/12, 150 pp.

Ichikawa, S., Yasuga, H., Tosha, T., and Karasawa, H., 2000: Development of downhole pump binary cycle power generation using geothermal water. In: *Proceedings of World Geothermal Congress, Kyushu-Tohoku, Japan,* 1283–1288.

Kunaruk, U., 1991: Design and selection of deep well pumps for geothermal wells. Report 8 in: *Geothermal training in Iceland 1991. UNU-GTP*, Iceland, 51 pp.

Lagat, J.K., 2004: *Geology, hydrothermal alteration and fluid inclusion studies of the Olkaria Domes geothermal field, Kenya.* University of Iceland, MSc thesis, UNU-GTP, Iceland, report 1, 79 pp.

Monroy, A.F.P., 2013: Geothermal Binary Cycle Power Plant Principles, Operations and Maintenance. *37th Anniversary workshop, UNU-GTP, Iceland.*

Mwawasi, H.M., 2014: *Feasibility Study of Using a Downhole Pumping System in Menengai well MW-17 for Geothermal Utilization*, 38th Anniversary workshop, UNU-GTP, Iceland, http://www.grogtp.is.

Ngugi, P.K., 2012: *What does Geothermal Cost? The Kenya Experience*. Presented at the *"Short Course VII on Exploration for Geothermal Resources",* organized by UNU-GTP, GDC and KenGen, Lake Bogoria and Lake Naivasha, Kenya.

Novomet ESP calculator software, 2022: *Novomet group internet*, website, *https://www.novometgroup.com/products-services/artificial-lift/software/esp-calculator/*